International Journal of Pharmaceutics: X 9 (2025) 100333

Contents lists available at ScienceDirect

International Journal of Pharmaceutics: X

journal homepage: www.sciencedirect.com/journal/international-journal-of-pharmaceutics-x

Terconazole loaded edge-activated hybrid elastosome for revamped corneal permeation in ocular mycosis: In-vitro characterization, statistical optimization, microbiological assessment, and in-vivo evaluation.

Sadek Ahmed [a], Michael M. Farag [a,*], Heba Attia [b], Bander Balkhi [c], Islam M. Adel [a], Asmaa Ashraf Nemr [a]

[a] Department of Pharmaceutics and Industrial Pharmacy, Faculty of Pharmacy, Cairo University, Cairo 11562, Egypt
[b] Department of Microbiology and Immunology, Faculty of Pharmacy, Cairo University, Cairo 11562, Egypt
[c] Department of Clinical Pharmacy, College of Pharmacy, King Saud University, Riyadh, Saudi Arabia

ARTICLE INFO

Keywords:
Terconazole
Hybrid elastosome
Edge activator
Ocular mycosis
Biofilm inhibition
Corneal permeation

ABSTRACT

Herein, we investigated the preparation and characterization of Terconazole loaded edge-activated hybrid elastosome (TCN-EHE) adopting thin film hydration technique for the treatment of ocular mycosis. Terconazole (TCN) is a broad spectrum antimycotic agent suffering from sparse aqueous solubility impeding its use in ophthalmic preparations. The scrutinized formulation variables namely X_1: Surfactant: Edge activator ratio (SAA: EA), X_2: Pluronic® L121 contribution (% of total SAA) and X_3: EA concentration (%*w/v*) were optimized adopting D-optimal design. Ten runs were prepared and characterized regarding their entrapment efficiency, particle size, polydispersity index and zeta potential. An optimized formula was generated, with high desirability, exhibited satisfactory entrapment efficiency, nanoscaled particle size aligning with TEM, plausible zeta potential and bi-phasic release pattern which were not altered after short-term storage. The optimized TCN-EHE displayed 1.94-fold enhanced ex-vivo corneal permeation flux. Safety was ratified through measured corneal hydration level, pH and histopathological evaluation. In-vivo corneal uptake visualized by confocal laser microscopy demonstrated 2.7-fold deeper penetration. Moreover, Superior antifungal activity has been demonstrated displaying 37 % bigger zone of inhibition, 8-fold lower minimum inhibitory and minimum fungal concentration alongside significantly higher biofilm inhibition activity at all tested concentrations for the optimized TCN-EHE compared to TCN suspension. Conclusively, we could prospect that TCN-EHE might be a revamped therapeutic alternative for the delivery of poorly soluble antimycotic agents for the combat of ocular mycosis.

1. Introduction

Oculomycosis or mycotic keratitis is considered as an eminent threat, presenting itself as a grave affliction of the cornea, second to cataract, with the potential to cause blindness (Singh et al., 2015). Regrettably, it ranks among the foremost causes of microbial keratitis or corneal ulceration. Recent conservative estimates indicate an alarming surge of nearly 1.5 million fresh cases annually (Brown et al., 2021), a figure consistent with projections made over two decades ago (Whitcher et al., 2001). Infections are often linked to the administration of steroids, ocular surface ailments, past ocular procedures, the wearing of contact lenses, and health conditions escorted with compromised immunity (Qiao et al., 2020).

Such fungal infection is casting its shadow over tropical and subtropical regions, where it manifests in up to 60 % of mycotic keratitis instances, likely attributable to humid temperate climate (Bongomin et al., 2017) and the prevalence of agricultural activities predisposing individuals to ocular trauma (Leck et al., 2002). Intriguingly, even amidst developing nations, fungal keratitis maintains its status as a disease rooted in socioeconomic disparity, with instances commonly linked to contact lens usage among individuals from impecunious backgrounds (Brown et al., 2021).

Antifungal medications suitable for treating fungal keratitis are broadly categorized into four primary groups: polyenes, azoles,

* Corresponding author at: Department of Pharmaceutics and Industrial pharmacy, Faculty of Pharmacy, Cairo University, Kasr El-Aini Street, Cairo 11562, Egypt.
E-mail address: michael.farag@pharma.cu.edu.eg (M.M. Farag).

https://doi.org/10.1016/j.ijpx.2025.100333
Received 9 March 2025; Received in revised form 4 April 2025; Accepted 6 April 2025
Available online 8 April 2025

allylamines, and echinocandins (Al-Badriyeh et al., 2010). Terconazole (TCN), a triazole ketal derivative, is a broad spectrum antimycotic agent with proven efficacy against a diverse array of yeasts and mycelial fungi. This potent antimycotic agent prohibits the morphogenetic transition of *Candida albicans* into its highly contagious pseudomycelium form. Terconazole has sparse aqueous solubility (0.08 ± 0.01 mg/mL in PBS pH 7.4, 2.75 ± 0.14 mg/mL in PBS pH 5.5, log P = 5.37 and pKa = 8) impeding its application in ocular formulations (Elnaggar et al., 2016; Zaghloul et al., 2022b). Nevertheless, literature screening showed several attempts to use terconazole for ocular delivery, including the development of silica/chitosan nanoparticles (Zaghloul et al., 2022a), PLGA microparticles (Zaghloul et al., 2022b), bilosomes (Abdelbary et al., 2016), integrated bilosome/self-nanoemulsifying system (Yousry et al., 2020) and cationic polymeric nanoparticles (Mohsen, 2022).

Topical administration, most commonly as eye drops, is preferred for the delivery of antimycotic agents for the treatment of fungal keratitis (Al-Badriyeh et al., 2009). This preference arises from its ease of application, minimal invasiveness, swift onset of action, affordability, minimal systemic adverse effects, and patient's acceptance (Davies, 2000). However, the effectiveness of conventional eye drops is limited by the tight junctions of cornea's epithelium, blinking and pre-corneal metabolism (Ding et al., 2018; Gaudana et al., 2010; Mannermaa et al., 2006). Lacrimation, a natural physiological hydration mechanism, resulted in dilution of the tear film, causing up to 10-fold reduction of ocular drug concentration. Therefore, conventional eye drops tend to have short residence time and diminished ocular bioavailability not exceeding 5 % (Casey-Power et al., 2022).

Elastosomes represent a modulated paragon of their traditional ancestor liposome predominantly composed of phospholipids, complemented by edge activators (EA) (Nemr et al., 2023). The EA is added to impart an elastic deformable nature by lowering the vesicles' surface tension allowing them to squeeze through interstitial spaces for deeper penetration through biological membranes without compromising vesicles' integrity (Aziz et al., 2023; Barbalho et al., 2024; Basha et al., 2013; Duangjit et al., 2013; Rathod et al., 2021; Srivastava et al., 2023). This composition is especially coinciding the complex structure of the corneal tissue, characterized by a lipophilic epithelium and a hydrophilic stroma (Cholkar et al., 2013). Aqueous dispersions of these nanovesicles amalgamate the benefits of robust physicochemical stability and ease of application. Consequently, they facilitate the effective penetration and sustained delivery of laded cargo, thereby enhancing therapeutic outcomes.

Lipid-based nanovesicular systems were modulated by replacing the lipid portion (phospholipids or cholesterol) with non-ionic SAA with low HLB like spans to form a more elastic paragon known as 'spanlastics'. We speculated that the use of a hybrid mixture of non-ionic SAA composed of a low HLB component (Pluronic® L121) as a vesicles' building unit alongside a high HLB component (Brij® 35) to distort the compact packing of the vesicles to impart a fluidizing nature in addition to the malleable effect of EA (Cremophor® RH 40) to produce ultra-deformable hybrid elastosomes while pertaining high %EE.

Drawing from the preceding discourse, our aim was to develop Terconazole loaded edge-activated hybrid elastosomes (TCN-EHE) using a hybrid mixture of non-ionic surfactants (Brij® 35 and Pluronic® L121) for stabilization of elastosomes coupled with Cremophore® RH 40 as edge activator to impart elastic deformability on the produced vesicles. D-optimal design was embraced to probe the significance of the following independent variables derived from a pre-formulation screening study namely, X_1: Surfactant: Edge activator ratio (SAA: EA), X_2: Pluronic® L121 contribution (% of total SAA) and X_3: EA concentration (%*w/v*) on the measured dependent responses including Y_1: Entrapment efficiency (%), Y_2: Particle size (nm), Y_3: Polydispersity index and Y_4: Zeta potential (mV). The optimized formula, generated by numerical optimization algorithms, was further evaluated regarding in-vitro release profile, storage stability and ex-vivo corneal permeation study compared to TCN suspension. Furthermore, the safety of the prepared system was scrutinized through histopathological examination, corneal hydration level and pH measurements to assure the safety of instillation. In-vivo performance was also evaluated by determining in-vivo corneal uptake through confocal laser microscopy and an array of microbiological assessments.

2. Materials and methods

2.1. Materials

Terconazole (TCN) was gifted as free sample from Marcyrl Pharmaceutical Industries, Egypt. Cremophor® RH 40 (polyoxyl 40 hydrogenated castor oil USP/NF) was procured from BASF, Germany. Cholesterol, Brij® 35 (polyoxyethylene (23) lauryl ether), Pluronic® L121 and dialysis membrane (Molecular weight cutoff 14,000 Da) were purchased from Sigma-Aldrich® (St. Louis, MO, USA). Methanol, chloroform, potassium dihydrogen phosphate, disodium hydrogen phosphate, potassium chloride and sodium chloride were obtained from El-Nasr Pharmaceutical Chemicals Co. (Cairo, Egypt). All additional chemicals and reagents utilized were of analytical reagent quality.

2.2. Animals

Male adult albino rabbits, with an average weight of 2.4 ± 0.32 kg, were individually housed in cages maintained at 25 ± 2 °C, with an alternating 12-h light/dark cycle. They were provided with standard commercial food and tap water. Before the commencement of the study, a preliminary examination of all rabbits' eyes was conducted, and only those without any signs of ocular inflammation were included. This research was approved by the Research Ethics Committee (REC) of the Faculty of Pharmacy, Cairo University, with approval number PI 3505. We have adhered to the guidelines outlined in the Guide for Care and Use of Laboratory Animals, as published by the US National Institute of Health (NIH Publication No. 85–23, revised 2011).

2.3. Preparation of Terconazole loaded edge-activated hybrid elastosomes (TCN-EHE)

Terconazole loaded edge-activated hybrid elastosomes (TCN-EHE) were fabricated adopting thin film hydration technique (Aziz et al., 2018) with few modifications. In brief, 10 mL of chloroform: methanol in a ratio (7:3) were added in a round-bottom flask to dissolve accurate weights of TCN (10 mg), cholesterol (50 mg) together with Cremophor® RH 40 as edge activator (either 0.05 or 0.1 % *w/v*) alongside a hybrid mixture of non-ionic surfactants (Pluronic® L121 and Brij® 35 either as 30: 70 or 60: 40), the added amount of SAA is based on SAA: EA ratio (7.5: 1 or 15: 1). The flask was attached to rotary evaporator (Hei-VAP Expert Heidolph Instruments GmbH & Co., Schwabach, Germany), it was conditioned at 60 °C and allowed to rotate at 90 rpm under reduced pressure for 15 min till the complete evaporation of the organic solvents. After that, a homogenous thin film is developed by the end of evaporation stage. Then, after releasing the vacuum pressure, 10 mL of double distilled water was added and the flask resumed rotation at the same speed at room temperature for another 15 min till the formation of milky dispersion of elastosomes. Consequently, the elastosomal dispersion was sonicated for 20 min in a bath sonicator (Ultrasonic bath sonicator, Model SH 150–41, MTI Corporation, Richmond, CA) at room temperature. Finally, the prepared dispersions were refrigerated at 4 °C to allow vesicles' maturation overnight before characterization.

2.4. Statistical design

The D-optimal design was selected to statistically refine the chosen independent variables namely, X_1: Surfactant: Edge activator ratio (SAA: EA), X_2: Pluronic® L121 contribution (% of total SAA) and X_3: EA concentration (%*w/v*). The scrutinized dependent responses were set to

Table 1
The probed independent variables of the D-optimal design and the applied constraints for optimization.

Factors (independent variable)	Level	
	-1	+1
X_1: SAA[a]: EA[b]	7.5	15
X_2: Pluronic® L121 contribution (% of total SAA)	30	60
X_3: EA concentration (%*w/v*)	0.05	0.1
Response (dependent variable)	Desirability constraints	
Y_1: Entrapment efficiency (%)	Maximize	
Y_2: Particle size (nm)	Minimize	
Y_3: Polydispersity index	Minimize	
Y_4: Zeta potential (mV)	Maximize (as absolute value)	

SAA[a], Surfactant; EA[b], Edge activator.

be, Y_1: Entrapment efficiency (%), Y_2: Particle size (nm), Y_3: Polydispersity index and Y_4: Zeta potential (mV) as listed in Table 1. The Design Expert® software (Version 12, Stat-Ease Inc., MN, USA) was utilized to generate 10 formulae representing the design space, their detailed composition is shown in Table 2. Subsequently, we have modulated the resulted polynomial equations by omitting non-significant model terms for better assessment of the relationship between the investigated factors and the measured responses. Also, we have outlined suggested restraints on the desired responses to allow the software, through numerical desirability algorithms, to derive an optimized formula (Farag et al., 2023).

2.5. In-vitro characterization of TCN-EHE

2.5.1. Calculation of percentage entrapment efficiency (%EE)

The indirect approach was adopted in the calculation of the percentage entrapment efficiency of the prepared TCN-EHE (Abdelbary et al., 2016). Briefly, an aliquot (1 mL) of elastosomal dispersion was ultracentrifuged (Sigma 3–30 KS cooling ultracentrifuge, Sigma Laborzentrifugen GmbH, Osterode am Harz, Germany) for 1 h at 22000 rpm under cooling conditions (4 °C). Then, the unentrapped TCN in the supernatant was measured spectrophotometrically (λ_{max} = 254 nm) after dilution 10 times with methanol (Shimadzu UV-1601 PC spectrophotometer, Kyoto, Japan) (Abdelbary et al., 2016). TCN concentration was determined against plain elastosomal dispersion as blank. The results of %EE are expressed as (mean ± SD) of three independent experiments. The following equation was used:

$$\%EE = \frac{Total\ theoretical\ TCN - unentrapped\ TCN}{Total\ theoretical\ TCN} \times 100$$

2.5.2. Determination of particle size (PS), polydispersity index (PDI) and zeta potential (ZP)

The PS and PDI of TCN-EHE were determined at 25 °C ± 2 °C, an aliquot of elastosomal dispersion (0.1 mL), diluted 100 times with double distilled water, to achieve adequate scattering intensity measured using Zetasizer Nano ZS (Malvern instruments; Worcestershire, UK). The technique is founded on dynamic light scattering caused by stochastic motion of the vesicles in the dispersion. Also, the ZP was measured using the same apparatus based on the vesicles' electrophoretic motion using an integrated helium-neon beam (at 633 nm) (Hussein et al., 2024; Fahmy et al., 2025). Results of PS, PDI and ZP were measured in triplicates.

2.6. Statistical optimization

Statistical optimization was applied, through numerical desirability function, on the design generated by Design Expert® software. The optimization was delineated by the applied constraints on the targeted responses, as mentioned in Table 1. The suggested optimized formula was prepared and re-evaluated regarding %EE, PS, PDI and ZP. To impartially evaluate the validity of the chosen model, one-way ANOVA analysis was performed to objectively verify the significance of the difference existed between the mean of the actual and predicted value for each corresponding dependent response (Habib et al., 2018).

2.7. Characterization of the optimized formula

2.7.1. Comparative in-vitro release study

The in-vitro release profiles of TCN-EHE, in comparison to TCN suspension (1 mg/mL), adopting dialysis bag technique (Weng et al., 2020). A Spectra Por® dialysis membrane (cutoff of 12,000–14,000 Da) was preconditioned overnight in the release medium. Subsequently, a precisely measured quantity of either TCN-EHE dispersion or TCN suspension, equivalent to 1.5 mg of TCN, was loaded into the dialysis bag, constituting the donor compartment. The dialysis bag was hermetically sealed and immersed within stoppered glass bottles containing 50 mL of pH 7.4 PBS with 20 % methanol (80:20 % *v*/v), representing the receptor compartment. These bottles were then positioned in a shaking water bath set at 37 ± 0.5 °C and operated at 60 strokes per minute (Unimax, IKA, Staufen, Germany) (Shahab et al., 2020). At predetermined intervals (0, 0.5, 1, 2, 4, 6, 8 h), samples of 1.5 mL were withdrawn from the receptor compartment, with equivalent volumes of fresh release medium introduced to maintain sink condition. These samples were subjected to spectrophotometric analysis at 254 nm to determine the percentage of TCN released at various time points. The depicted release profiles are derived from the average values obtained from three experimental replicates.

The in-vitro release profiles were kinetically analyzed by fitting in zero order, first order, Higuchi's diffusion and Korsmeyer-Peppas models' equations. Then, the regression coefficient (R^2) was calculated for each model. The model with higher regression coefficient was selected to best describe the release kinetics of the optimized formula (Tawfik et al., 2023).

Table 2
Composition and characterization of TCN-EHE adopting D-optimal design (*n*=3, mean ± SD).

Formulae	X_1: SAA[a]: EA[b]	X_2: Pluronic® L121 (% of SAA)	X_3: EA conc. (%w/v)	Y_1: EE[c] (%)	Y_2: Particle size (nm)	Y_3: PDI[d]	Y_4: Zeta potential (mV)
T1	7.5	30	0.05	73.51 ± 3.15	195.1 ± 0.85	0.358 ± 0.02	−22.4 ± 0.57
T2	7.5	30	0.05	75.42 ± 1.36	197.7 ± 3.54	0.452 ± 0.05	−23.9 ± 4.38
T3	7.5	30	0.05	79.15 ± 1.62	205.3 ± 0.14	0.334 ± 0.04	-24.4 ± 2.40
T4	7.5	60	0.05	85.97 ± 1.48	227.4 ± 0.21	0.314 ± 0.06	−25.4 ± 1.63
T5	7.5	30	0.1	75.42 ± 1.36	247.7 ± 1.13	0.285 ± 0.01	−28.9 ± 0.21
T6	7.5	60	0.1	87.16 ± 1.66	255.3 ± 3.39	0.271 ± 0.03	−30.6 ± 1.91
T7	15	30	0.05	82.54 ± 0.84	227.1 ± 4.74	0.311 ± 0.05	−31.1 ± 3.54
T8	15	60	0.05	91.45 ± 2.19	232.9 ± 1.48	0.348 ± 0.03	−31.4 ± 0.28
T9	15	30	0.1	81.05 ± 3.22	250.1 ± 4.6	0.348 ± 0.04	−33.2 ± 3.54
T10	15	60	0.1	89.57 ± 1.8	256.1 ± 1.06	0.256 ± 0.01	−33.4 ± 2.83

SAA[a], Surfactant; EA[b], Edge activator; EE[c], Entrapment efficiency; PDI[d], Polydispersity index.

2.7.2. Corneal ex-vivo permeation study

Corneal samples were sourced from mature male albino rabbits. The rabbits were anesthetized using an IM combination of ketamine (200 mg/kg) and xylazine (20 mg/kg) (Eldeeb et al., 2019; Sayed et al., 2020). Subsequently, euthanasia was performed through decapitation. Following euthanasia, the eyeballs were promptly removed, and the corneas were carefully dissected from the globes. These excised corneas underwent meticulous cleansing with saline solution to ensure the absence of any wrinkles or folds that could compromise the integrity of the membrane prior to mounting. Utilization of the transparent corneas in permeation experiments was initiated within 30 min following the sacrifice of the animals (Dai et al., 2013).

Corneal ex-vivo permeation study of TCN was conducted, as three independent experiments, using a Franz diffusion cell (Hanson Research in Chatsworth, USA) featuring both a donor and a receptor compartment. The donor compartment was filled with 1.5 mL of TCN-EHE or TCN suspension (1 mg/mL) (Farag et al., 2023; Nemr et al., 2022). Simultaneously, the receptor compartment was loaded with 25 mL of freshly prepared simulated tear fluid adjusted to pH 7.4. A plastic membrane was utilized to secure the cornea, ensuring a constant surface area for diffusion (0.785 cm^2). The membrane, bearing the cornea, was positioned between the two compartments. The cells were maintained at 37 ± 0.2 °C and stirred at 50 rpm with a magnetic stirrer. Samples were withdrawn from the receptor compartment at predetermined intervals (0, 1, 2, 4, 6, 8, 10 h), with each withdrawn aliquot of 2 mL being immediately replaced with fresh media. Samples underwent filtration through a 0.22 μm nylon filter prior to measurement against a blank solution comprising the release medium. The cornea was mounted in this medium but lacking any applied formula, blank samples were withdrawn at the same predetermined time intervals. The concentration of TCN was subsequently determined spectrophotometrically at 254 nm (ElMeshad and Mohsen, 2016; Kouchak et al., 2019). The cumulative amount of drug permeated per unit area (mg/cm^2) was plotted against time (h). The maximum flux (J_{max}) at 10 h and the enhancement ratio (ER) were computed using specified equations (Younes et al., 2018):

$$Jmax = \frac{Amount\ of\ drug\ permeated}{Time \times area\ of\ membrane}$$

$$ER = \frac{Jmax\ of\ TCN - EHE}{Jmax\ of\ TCN\ suspension\ (control)}$$

2.7.3. Corneal hydration level

Following the corneal ex-vivo permeation study, corneal hydration level was measured to assess corneal tissues damage during the permeation study (Liu et al., 2011). Such parameter is critical to evaluate the damage occurred during ex-vivo permeation study (Liu et al., 2005). The damage might be caused by incorrect handling of excised corneal tissues or the applied formula to validate that the results from ex-vivo permeation study were obtained using intact corneal tissues. Each cornea was taken out and cleaned to get rid of any remaining surface's residues, dried with a filter paper to remove extra water, and then weighed initially (W_i). Later, it was allowed to dry at 50 °C for one day and re-weighed (W_f). The percentage corneal hydration level (%HL) was calculated using the following equation (Moustafa et al., 2017):

$$\%HL = \left[1 - \left(\frac{Wi}{Wf}\right)\right] \times 100.$$

2.7.4. Effect of short-term storage

Short-term storage was conducted to detect any changes that might occur under specific conditions. The optimized formula was stored for 3 months in a stoppered vial and kept refrigerated at 5 ± 3 °C. After this time, the measured responses were assessed again including, %EE, PS and ZP. One-way ANOVA, using SPSS software version 26.0 (SPSS Inc. in Chicago, IL, USA), was performed to investigate the presence of any significant changes during storage. Furthermore, the in-vitro release study was repeated, and a similarity factor was calculated to check the presence of significant difference regarding the release pattern of the optimized formula before and after storage using the following equation (Nemr et al., 2021; Sayed et al., 2021):

$$f_2 = 50.\log\left\{\left[1 + \left(\frac{1}{n}\right)\sum_{t=1}^{n}(R_t - T_t)^2\right]^{-0.5}.100\right.$$

The percentages of TCN released before and after the storage period are denoted as R_t and T_t respectively. A value exceeding 50 is necessary to validate the similarity between the release profiles.

2.7.5. Transmission electron microscopy (TEM)

The morphological shape of the optimized TCN-EHE was illustrated using TEM (Joel JEM 1400, Tokyo, Japan). In brief, the elastosomal dispersion was diluted with double distilled water (20 times) and filtered to remove any aggregates. Consequently, an aliquot (0.1 mL) of the dispersion was mixed with 1 % phosphotungstic acid. Then, a carbon-coated copper grid was impregnated in the mixture and the grid was dried to drain excess sample at ambient temperature prior to examination step (Elgendy et al., 2024; Shahab et al., 2020).

2.7.6. Fourier-transform infra-red spectroscopy (FTIR)

The FT-IR spectra of individual components, alongside the optimized TCN-EHE were analyzed using an FTIR spectrophotometer (Bruker model 22, Coventry, UK). An accurate weight (3 mg) of each component was blended with dry potassium bromide and molded into a disc before undergoing scanning in the range of 4000–500 cm^{-1} at ambient temperature (Younes et al., 2018).

2.8. Safety evaluation

2.8.1. pH measurement

The pH measurement is crucial to assess the safety and tolerability of ophthalmic preparations (Sayed et al., 2021). It is recommended that the pH of ophthalmic products oscillate between 3.5 and 8.5 to avoid irritation and excessive lacrimation which tend to wipe out applied formulations (Alhakamy et al., 2022; Jesus et al., 2022; Pharmacopeia, 2021). The pH of the optimized formula was measured in triplicates using Jenway pH meter (model-3505, Bibby Scientific Ltd., UK), the results were expressed as mean ± SD.

2.8.2. Histopathological evaluation

Six male albino rabbits were used for histopathological evaluation. Before study initiation, the rabbits were visually inspected to ensure the absence of any signs of redness or inflammation. Our objective was to detect any histopathological changes in the rabbits' eyes following the application of TCN-EHE. An aliquot (0.1 mL) of the optimized TCN-EHE was instilled three times daily for one week into the right eye's cul-de-sac of rabbits. Normal saline was instilled to the left eye as negative control. By the end of the study, the rabbits were euthanized, their eyeballs were removed, washed with PBS (pH 7.4), and preserved in 10 % formalin saline solution until further analysis.

Subsequently, the tissues underwent dehydration using serial alcohol dilutions, followed by immersion in xylene and embedding in paraffin blocks at 56 °C for one day. Tissue sections of 4 μm thickness were then prepared using a rotary microtome (Leica Microsystems SM2400, Cambridge, UK). These sections were stained with hematoxylin and eosin to be mounted on glass slides prior to examination using light microscope (Leica Imaging Systems Ltd., Cambridge, England) (Abdellatif et al., 2022).

2.9. Efficacy evaluation of the optimized TCN-EHE

2.9.1. In-vivo corneal uptake using Confocal Laser Microscopy (CLM)

Confocal Laser microscopy (LSM 710; Carl Zeiss, Jena, Germany) was used to examine the optimized formula prepared using Rhodamine B (RhB) at a concentration of 0.1 % *w*/w instead of TCN. The right eye of male albino rabbits was used to instill 100 µL of RhB-EHE, while the left eye served as negative control receiving only an equivalent volume of RhB-solution. Following a 6-h interval, the rabbits were euthanized. The transparent corneas were delicately excised, and the debris were removed, with the corneal tissues subsequently preserved in artificial tears for immediate imaging. RhB fluorescence was measured through excitation at 485 and 595 nm using argon and helium-neon lasers, respectively. Confocal images were meticulously processed utilizing LSM software version 4.2 (Carl Zeiss Microimaging, Jena, Germany) (Younes et al., 2018).

2.9.2. Determination of the antifungal activity using Kirby–Bauer disk diffusion susceptibility test

Fungal inocula were prepared by picking 2–5 distinct colonies from 24-h-old culture of *Candida albicans* ATCC 60193 on Sabouraud Dextrose Agar (SDA). Colonies were suspended in sterile saline and the turbidity of the resulting suspension was adjusted to 0.5 McFarland standard at 550 nm wavelength. Sterile cotton swabs were dipped into the turbidity-adjusted fungal suspension, within 15 min of adjusting the turbidity, and rotated several times. Then, we streaked the swabs over the entire dried surfaces of Muller-Hinton agar plates that were supplemented with 2 % glucose and 0.5 µg/mL methylene blue (Jayachandran et al., 2018).

Ten microliters (equivalent to 5 µg) of the optimized TCN-EHE and the TCN suspension were loaded on sterile filter paper discs (11 mm in thickness) and allowed to dry, then the dried loaded disks were then dispensed onto the surface of the inoculated plates and pressed down gently (Osman et al., 2023). The plates were finally incubated for 24 h at 37 °C, after which, the inhibition zones were measured in mm. The experiment was done in triplicate.

2.9.3. Determination of the minimum inhibitory concentration (MIC)

MIC and MFC values were employed because they are the accepted benchmarks for evaluating antifungal potency. Minimum inhibitory concentration was determined by the broth microdilution method according to the guidelines of the Clinical and Laboratory Standards Institute (CLSI, 2018). Two-fold serially diluted preparations of both TCN suspension and optimized TCN-EHE were prepared in a total volume of 100 µL double-strength Sabouraud Dextrose Broth (SDB) (500–0.122 µg/mL). The serially diluted preparations were dispensed into U-shaped bottom, sterile 96-well plates. Then, 10 µL of *Candida albicans* standard strain (ATCC 60193) suspension (inoculum size of 10^5–10^6 CFU/mL) was added to each well. Negative control (control for the sterility of the media) was performed by adding 100 µL double-strength SDB with neither fungal suspension nor any concentration of diluted drug preparation. Positive control (fungal growth control) was performed by adding 100 µL double-strength SDB without any concentration of diluted drug preparation then adding 10 µL of fungal inoculum.

The microtitre plates were incubated at 37 °C for 24 h. The microtitre plates were then examined both visually and by measuring the absorbance at a wavelength of 600 nm in a 96-well plate reader. The MIC was determined as the lowest concentration showing no observable fungal growth. Biological and technical triplicates of the experiment were conducted ($n = 9$).

Table 3
Summary of regression coefficients of model responses alongside related significant factors.

Response	R^2	Adjusted R^2	Predicted R^2	Adequate precision	Significant factors
Y_1: EE[a] (%)	0.9369	0.9189	0.8860	15.172	X_1, X_2
Y_2: PS[b] (nm)	0.9018	0.8527	0.7341	10.637	X_2, X_3
Y_3: PDI[c]	0.4743	0.2115	−0.2796	3.1912	–
Y_4: ZP[d] (mV)	0.9096	0.8838	0.8111	12.835	X_1, X_3

Abbreviations: EE[a], entrapment efficiency; PDI[b], poly dispersity index; PS[c], particle size; ZP[d], zeta potential.

2.9.4. Determination of the minimum fungicidal concentration (MFC)

For both preparations (drug suspension and optimized formula), the determination of MFC was performed by broth microdilution technique according to the Clinical and Laboratory Standards Institute guidelines (CLSI, 2018). Briefly, Two-fold serially diluted preparations of both the TCN suspension and optimized TCN-EHE (at concentrations greater than the calculated MIC) together with the 10 µL fungal inoculum suspension (inoculum size of 10^5–10^6 CFU/mL) were incubated in 96-well plates at 37 °C for 24 h. Then, 10 µL of each well's mixture was spotted on SDA plates. The plates were then incubated at 37 °C for another 24 h. The SDA plates were then examined visually, and the MFC was expressed as the lowest concentration that shows no visible fungal growth. Biological and technical triplicates of the experiment were conducted (n = 9).

2.9.5. Testing the effect of the optimized TCN-EHE on biofilm formation by the crystal violet method

The changes in the biofilm formed by the tested *Candida albicans* strain in the presence of TCN (either as TCN suspension or optimized TCN-EHE) were determined as described in (Haney et al., 2021; O'Toole, 2011). Briefly, the turbidity of an overnight culture of *Candida albicans* ATCC 60193 was adjusted by dilution with double-strength SDB to $O{\cdot}D_{600}$ of 1, followed by 100-fold dilution. An equal volume of the adjusted fungal inoculum and either TCN suspension or optimized TCN-EHE were loaded in sterile 96-well non pyrogenic polystyrene culture flat-bottom plates (total volume = 100 µL/well), so the final drug concentrations in the wells represent $^1/_8$, ¼, ½, 1, 2, and 4 X where X is the calculated MIC. Plates were statically incubated at 37 °C for 24 h. Negative, positive, and color controls were performed.

After incubation, the absorbance of the planktonic growth was measured at $O{\cdot}D_{600}$ by an automated spectrophotometric plate reader (Biotek, Synergy 2, USA), then the supernatant was gently removed, and the wells were washed twice with sterile phosphate-buffered saline (PBS). The plates were left to dry thoroughly then the formed biofilm was stained with 125 µL 0.5 % *w/v* aqueous solution of crystal violet for 30 min at room temperature. The excess of crystal violet was then removed by washing the plates three times with sterile distilled water and the plates were left to dry completely.

The crystal violet dye bound to the cells was extracted by addition of 150 µL 95 % w/v ethanol and incubation for 15 min with shaking at 110 rpm. Finally, the absorbance at a wavelength of 570 nm was measured by the automated spectrophotometric plate reader Synergy 2. Normalization was done by dividing OD_{570} by OD_{600} of the planktonic cultures. The experiment was done in technical triplicates and repeated three times as biological independent replicates. The biofilm inhibition % was calculated using the following equation:

$$Biofilm\ inhibition\% = \frac{OD\ Control - OD\ Test}{OD\ Control} \times 100$$

3. Results and discussion

Terconazole loaded edge-activated hybrid elastosomes were successfully fabricated adopting thin film hydration technique following a D-optimal design. The formulae were evaluated regarding their entrapment efficiency, particle size, polydispersity index, and zeta potential to generate an optimized formula for further characterization and

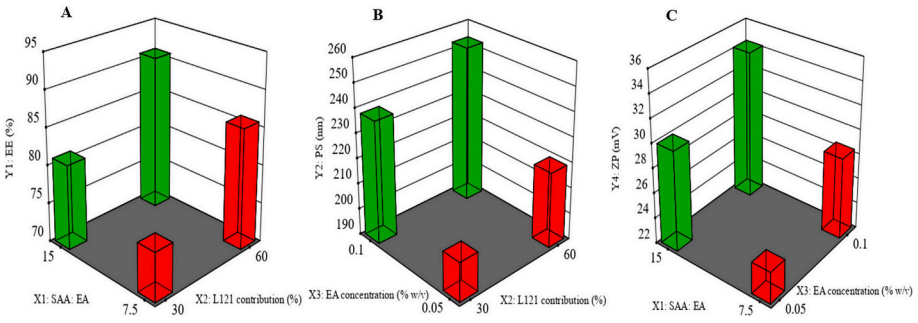

Fig. 1. A: 3D plot showing the effect of surfactant: edge activator ratio and Pluronic® L121 (% of surfactant mixture) on the entrapment efficiency of TCN-EHE. B: 3D plot showing the effect Pluronic® L121 (% of surfactant mixture) and edge activator concentration (%w/v) on the particle size of TCN-EHE. C: 3D plot showing the effect of surfactant: edge activator ratio and edge activator concentration (%w/v) on the zeta potential of TCN-EHE.

evaluation.

3.1. In-vitro characterization of TCN-EHE

3.1.1. Model analysis of %EE

An ocular system should have high entrapment efficiency, an imperative feature to circumvent corneal intricacies and foster better absorption and bioavailability (Abdelbary et al., 2016). The calculated %EE of the prepared TCN-EHE fluctuated between 73.51 % ± 3.15 % and 91.45 % ± 2.19 % as shown in Table 2. ANOVA analysis showed that both X_1: SAA: EA ratio and X_2: Pluronic® L121 (% of SAA) have a significant effect on %EE as summarized in Table 3.

The SAA: EA ratio was found to have a significant positive impact ($P = 0.0036$) on %EE as shown in Fig. 1A, denoting that increasing SAA: EA ratio from 7.5:1 to 15:1 resulted in increasing the entrapment efficiency from as low as T1 (73.51 % ± 3.15 %) up to T8 (91.45 % ± 2.19 %). Hydrophilic surfactants like Cremophor ® RH 40 (HLB ≈ 14–16) are typically used as edge activators (EA) to impart flexibility on vesicles' bilayer causing their destabilization (Kakkar and Pal Kaur, 2013). The magnitude of EA is dependent on their ratio and structure, higher ratio and bulky structure provide greater fluidizing impact contributing to lower entrapment of the resulting malleable vesicles. A comparative study between Cremophor® RH 40, Brij® 35 and Tween® 40 concluded that the bulky structure of Cremophor® RH 40 disturbed vesicles' packing and resulted in improper closure leading to leakage and poor entrapment (Al-Mahallawi et al., 2017; Rathod et al., 2021).

The positive impact of Pluronic® L121 (% of SAA) on %EE ($P < 0.0001$) is depicted in Fig. 1A, the increase of % Pluronic® L121 from 30 % to 60 % resulted in higher %EE, literature review concluded that the %EE of hydrophobic drugs like TCN (log $P = 5.37$) is enhanced by using hydrophobic SAA (Bnyan et al., 2018; Mahale et al., 2012; Taymouri and Varshosaz, 2016). Considering that Pluronic® L121 is a hydrophobic SAA (HLB ≈ 0.5) in contrast to the hydrophilic SAA Brij® 35 (HLB ≈ 16.9), thus, increasing the proportion of Pluronic® L121 on behalf of Brij® 35 will likely increase %EE. Similar results were obtained by Abdelbary et al. (Abdelbary et al., 2017) as they incorporated the hydrophobic drug ketoconazole in proniosomal gel where higher %EE was obtained with Pluronic® L121 systems relative to those containing Brij® 35. It was concluded that hydrophobic SAA as Pluronic® L121 are capable of becoming vesicular building unit with high %EE for systems containing cholesterol owing to their hydrophobic nature (Manosroi et al., 2003; Nemr et al., 2023) while hydrophilic SAA as Brij® 35 tend to act as solubilizer for cholesterol due to their hydrophilic nature resulting in lower %EE (Gorjian et al., 2021; Pardakhty et al., 2007).

3.1.2. Model analysis of particle size (PS) and polydispersity index (PDI)

Putatively, corneal penetration is endowed for laded cargo inside nano-sized vesicles (Dai et al., 2013). The particle size of the prepared TCN-EHE oscillated between 195.1 ± 0.85 to 256.1 ± 1.06 nm as demonstrated in Table 2. ANOVA analysis of the independent variables showed that X_2: Pluronic® L121 (% of SAA) and X_3: EA conc. (%*w/v*) were significantly ($P = 0.047$ and 0.0013 respectively) affecting particle size as shown in Table 3.

The positive impact of Pluronic® L121 (% of SAA) on PS is illustrated in Fig. 1B, conveying that the higher the proportion of Pluronic® L121 on behalf of Brij® 35 the larger the PS of the resulting vesicles. A plausible explanation could be based on the hydrophobic nature of Pluronic® L121 (HLB ≈ 0.5) allowing more drug to be incorporated inside the hydrophobic milieu within the vesicles by creating accommodation spaces for the drug resulting in increased interlamellar distances within the lipid bilayer which could be correlated to the increased %EE caused by higher Pluronic® L121 proportion. Similar findings were observed by Aziz et al. (Aziz et al., 2022) and Nemr et al. (Nemr et al., 2021).

Regarding EA concentration, its positive impact on the PS is depicted in Fig. 1B, denoting that the increasing the concentration of EA from 0.05 to 0.1 (%*w/v*) will result in larger vesicles. Generally, hydrophilic surfactants, as Cremophor® RH 40 (HLB ≈ 14–16), tend to form larger vesicles since they have high surface free energy (Abdelkader et al., 2010). Similar findings by EL zaafarany et al. (El Zaafarany et al., 2010) as they claimed that vesicles growth occurred upon addition of EA till the concentration exceeded 15 % then a size reduction was observed.

The polydispersity index is calculated by dividing the standard deviation by the mean particle size. It is a measure of vesicles' homogeneity and reproducibility of method of preparation (Shakeel et al., 2007). The PDI of the prepared TCN-EHE ranged from 0.256 ± 0.01 to 0.452 ± 0.05 as summarized in Table 2. Since it is ratified that PDI < 0.3 is preferred we could deduce that the prepared systems showed unimodal symmetrical pattern of distribution (ElMeshad and Mohsen, 2016). ANOVA analysis emphasized that investigated independent variables exhibited non-significant ($P > 0.05$) influence on PDI as summarized in Table 3, therefore, we decided to exclude it from the numerical optimization algorithms.

3.1.3. Model analysis of zeta potential (ZP)

The vesicles' surface charge is known as zeta potential, higher zeta potential is required to thwart particles aggregation through electric repulsion so it is considered as an indirect reflection of system stability (Ahmed et al., 2022). Through literature review, it was found that nanosystems should exhibit a zeta potential value ≥30 mV as absolute value to endow an acceptable stability (Al-Mahallawi et al., 2015; El Taweel et al., 2023). Herein, the zeta potential of the prepared TCN-EHE fluctuated between −22.4 ± 0.57 mV and − 33.4 ± 2.83 mV as mentioned in Table 2, so the prepared TCN-EHE formulae are prospected to exhibit plausible stability. Since all formulae exhibited negative zeta potential, the ZP data will be discussed in terms of absolute values to avoid misperception.

Only X_1: SAA: EA ratio and X_3: EA conc. (%*w/v*) exhibited a

Table 4
Comparison of the observed vs predicted responses of the optimum formula and effect of short-term stability.

Response		Y_1	Y_2	Y_4
		EE[a] %	PS[b] (nm)	ZP[c] (mV)
Observed value		91.45	232.85	31.40
Predicted value		91.02	232.11	30.95
% Deviation (absolute)		−0.48	0.32	1.45
Parameter	Fresh	Stored for 3 months at 4–8 °C		
		Value	Probability (*p*-value)*	
Y_1: EE[a] (%)	91.45 ± 2.19	87.95 ± 1.02	0.176	
Y_2: PS[b] (nm)	232.85 ± 1.48	236.85 ± 5.02	0.393	
Y_4: ZP[d] (mV)	−31.4 ± 0.28	−34.65 ± 1.77	0.124	

Abbreviations: EE[a], entrapment efficiency; PS[b], particle size; ZP[c], zeta potential.
* One-way ANOVA statistical analysis.

significant effect (P = 0.0006 and 0.0034 respectively) on ZP as concluded from ANOVA statistical analysis outlined in Table 3. Regarding SAA: EA ratio, it showed a positive impact on zeta potential as illustrated in Fig. 1C, conveying that increasing SAA: EA ratio the zeta potential tends to increase. Intriguingly, despite that the used SAA are non-ionic surfactants (Pluronic® L121, Brij® 35), it was found through literature review that many non-ionic surfactants (e.g. Tween 80) tend to impart a negative surface charge even higher than anionic surfactants (e.g. sodium cholate and deoxycholate) (El Zaafarany et al., 2010; ElMeshad and Mohsen, 2016), the acceptable reason for such phenomena is the preferential adsorption of hydroxyl ions rather than hydronium ions at the cholesterol/water interface in presence of non-ionic surfactants (Exerowa, 1969; Karraker and Radke, 2002).

Similarly, the EA concentration displayed a positive effect on zeta potential as depicted in Fig. 1C, indicating that increasing the EA concentration will increase the zeta potential. Despite that the EA (Cremophor® RH 40) is also categorized as non-ionic SAA, we believe that the same abovementioned reasons under SAA:EA ratio can be applied here.

3.2. Statistical optimization

The formulation variables scrutinized using a D-optimal design through the preparation and evaluation of suggested formulae generated by the Design expert® software. The numerical desirability algorithms were adopted to suggest an optimized formulation by setting constraints for the targeted responses as mentioned in Table 1. Obviously, our goals are to prepare a TCN-EHE system displaying high entrapment, small particle size, good homogeneity for efficient delivery of laded drug, and high zeta potential for optimum stability. Based on numerical desirability function, an optimized formula was suggested by the software with high desirability (0.871), the formula was composed of SAA: EA (15: 1), Pluronic® L121 (60 %) and EA (0.05 %w/v).

Consequently, the optimized formula was prepared and characterized to evaluate the percentage deviation between the actual versus predicted responses generated by the software as shown in Table 4. Statistical analysis using student *t*-test was performed and it showed non-significant ($P > 0.05$) difference between the actual and predicted responses of the optimized formula ratifying the validity of the optimization process.

3.3. Characterization of the optimum TCN-EHE

3.3.1. Comparative in-vitro release study

The in-vitro release profiles of the optimized TCN-EHE versus TCN suspension are illustrated in Fig. 2A. Kinetic analysis of the release pattern of the optimized TCN-EHE best fitted Higuchi's diffusion model ($r^2 = 0.997$ compared to first order $r^2 = 0.969$, zero order $r^2 = 0.966$ and Korsmeyer-Peppas $r^2 = 0.835$ where $n = 0.329$ corresponding to Fickian diffusion) similarly matching elastosomal formulations (Nemr et al., 2023; Shang et al., 2022). Thus, we could conclude that TCN was released by diffusion through lipid membrane (cholesterol) of elastosomal system which is highly stabilized by the Pluronic® L121 while hydrophilic SAA like Brij® 35 and EA facilitated drug release by disturbing the packing of cholesterol as discussed under Section 3.1.1. The release profile of the optimized TCN-EHE showed a bi-phasic release pattern characterized by an initial burst of rapid drug release where almost half of the dose 46.02 % ± 0.09 % were released only in the first 2 h compared to 21.73 % ± 0.83 % were released from TCN suspension ($P < 0.05$) followed by controlled release where the remaining of the dose 92.83 % ± 3.28 % were released after 8 h relative to only 49.49 % ± 0.85 % for TCN suspension ($P < 0.05$). Although the suspension seemed to have slower release than TCN-EHE, we should also consider the short residence time of ocular formulations entailing the need to expedite complete drug release without compromising the controlled release pattern to endow patient's compliance.

3.3.2. Corneal ex-vivo permeation study

The corneal ex-vivo permeation profiles of the optimized TCN-EHE relative to TCN suspension are depicted in Fig. 2B. Statistical analysis using student-*t*-test demonstrated that the optimized TCN-EHE exhibited statistically significant ($P < 0.05$) revamped permeation of TCN compared to TCN suspension reflected through the cumulative amount of drug permeated at 10 h (Q_{10h} = 555.57 ± 54.45 μg/cm^2 versus 285.80 ± 33.89 μg/cm^2 respectively). Another important parameter to evaluate the ex-vivo performance is the calculation of maximum flux (J_{max}) where the optimized TCN-EHE exhibited statistically significant ($P < 0.05$) higher (J_{max}) = 55.56 ± 5.45 μg/cm^2/h versus 28.58 ± 3.39

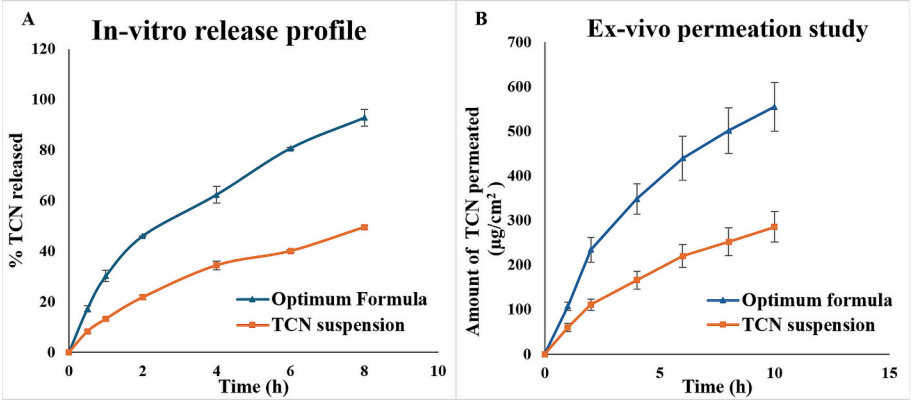

Fig. 2. A: In-vitro release profiles of the optimized formula of TCN-EHE and Terconazole suspension in 50 mL PBS (pH 7.4) with 20 % methanol (80:20 % *v*/v). B: Corneal ex-vivo permeation profiles of the optimized formula of TCN-EHE and Terconazole suspension in 25 mL simulated tear fluid (pH 7.4).

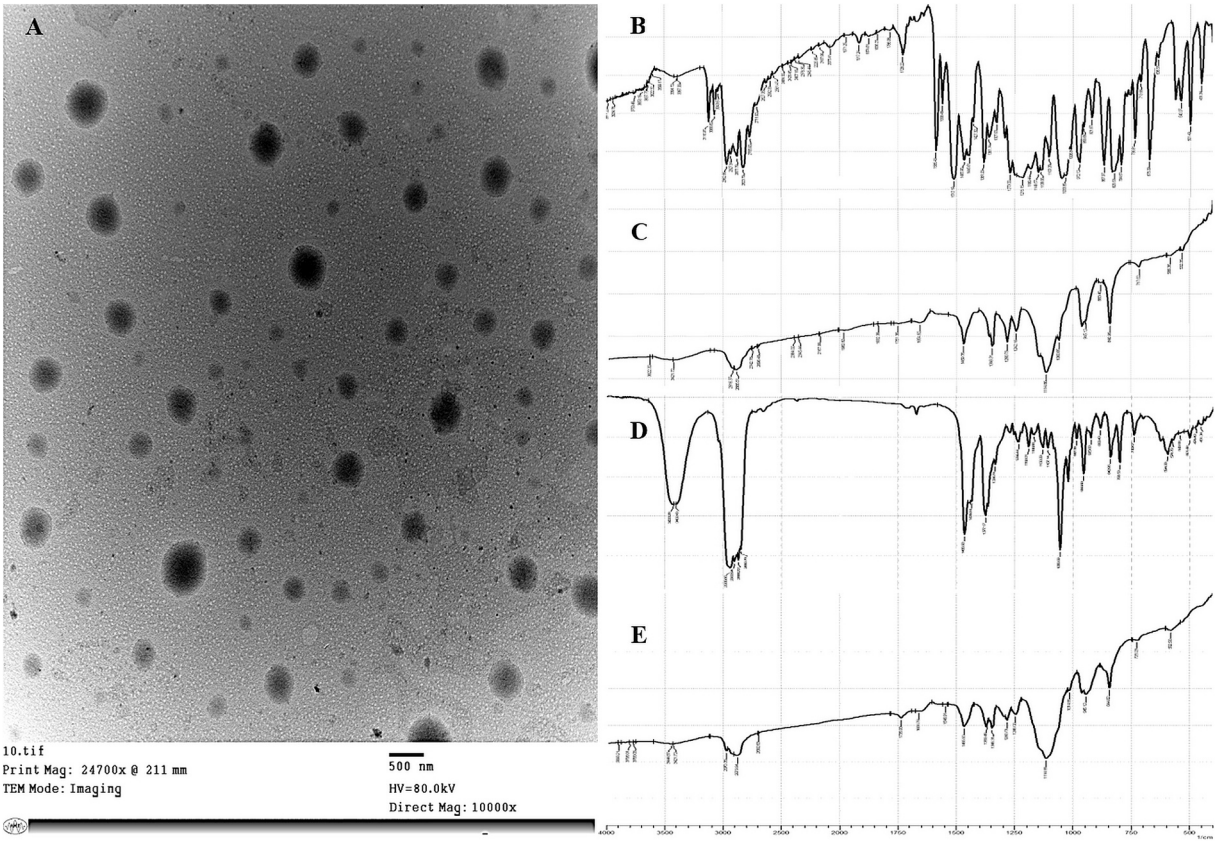

Fig. 3. A: Transmission electron micrograph of the optimized TCN-EHE dispersion (10,000× magnification and excitation═80 Kv). FTIR spectra of: B: Terconazole (TCN), C: Brij® 35, D: Cholesterol, E: TCN-EHE optimized formula.

μg/cm^2/h with an overall enhancement ratio = 1.94.

The demonstrated superior ex-vivo penetration of the optimized TCN-EHE could be ascribed to many factors including the use of hybrid mixture of SAA composed of lipophilic Pluronic® L121 as vesicles' building unit and hydrophilic SAA Brij® 35 in addition to Cremophor® RH 40 as EA, both Brij® 35 and Cremophor® RH 40 as hydrophilic SAA imparted an elastic nature on the vesicles' bilayer causing their destabilization and fluidity which allowed them to squeeze through corneal membrane tight junctions (El Zaafarany et al., 2010; Kakkar and Kaur, 2011; Kakkar and Pal Kaur, 2013). The corneal epithelium's tight junctions become loose as a collateral effect of the SAA (Ahmed et al., 2022; Younes et al., 2018). Cholesterol as a vesicles' component is also reported by Eldeeb et al. as a penetration enhancer facilitating vesicles' diffusion (Eldeeb et al., 2019).

Additionally, the nanoscaled size of the vesicles is reported to prolong corneal residence time allowing better diffusion through corneal stroma (Mosallam et al., 2021). Intriguingly, despite it is reported that corneal epithelium bears slight negative charge, the negative zeta potential aided in corneal permeation (Liang et al., 2023). Gonzalez et al. (Gonzalez-Pizarro et al., 2018) and Sanchez et al. (Sánchez-López et al., 2016) have reported that corneal drug penetration could be improved by negatively charged nanovesicles. Moreover, Abdelhakeem et al. (Abdelhakeem et al., 2021) demonstrated that negatively charged Eplerenone loaded nanostructure lipid carriers have superior permeation compared to their positively charged counterparts. Also, Quinteros et al. (Quinteros et al., 2016) have reported that negatively charged nanocapsules coated with ethyl cellulose exhibited better acetazolamide corneal ex-vivo permeation.

3.3.3. Corneal hydration level

To assess the presence of corneal injury following the conduction of ex-vivo permeation study, we have calculated the corneal hydration level. Normally, a healthy corneal hydration level should be ranged between 76 % and 80 % (Huang et al., 2017). The corneal hydration level following the ex-vivo permeation of the optimized TCN-EHE and TCN suspension was found to be 77.71 % ± 0.11 % and 78.18 % ± 0.91 % respectively. Statistical analysis using student t-test was performed and it showed non-significant ($P > 0.05$) difference between both treatments. Thus, emphasizing the possible safe application of the optimized formula (Moustafa et al., 2017).

3.3.4. Effect of short-term storage

By the end of 3 months storage period, the meticulous physical examination of stored vesicles did not observe any aggregates formation or change in their organoleptic properties. The measured %EE, PS and ZP for fresh and stored optimized formulae are summarized in Table 4. Statistical analysis using student t-test didn't find any significant difference ($P = 0.176$, 0.393 and 0.124 respectively) regarding the measured responses. Moreover, the similarity factor ($f2$) was calculated for the in-vitro release profile of fresh and stored formulae and was found to be 62.87, concluding that storage didn't affect the in-vitro release performance (Diaz et al., 2016). Based on the aforementioned qualities, we could speculate that the high of the optimized formula is ascribed to its high negative zeta potential (−31.4 ± 0.28 mV) expressed over its high surface area owing to its nanoscaled size causing electrostatic repulsion thus, preventing vesicles' agglomeration (Harisa and Badran, 2015).

3.3.5. Transmission electron microscopy (TEM)

Transmission electron microscopy serves as an indispensable tool for discerning the morphology and measuring the vesicular diameter of meticulously crafted nanostructures (Farag et al., 2021; Farag et al., 2024). This examination was undertaken to consolidate the findings acquired via dynamic light scattering (Ahmed et al., 2024b). As depicted

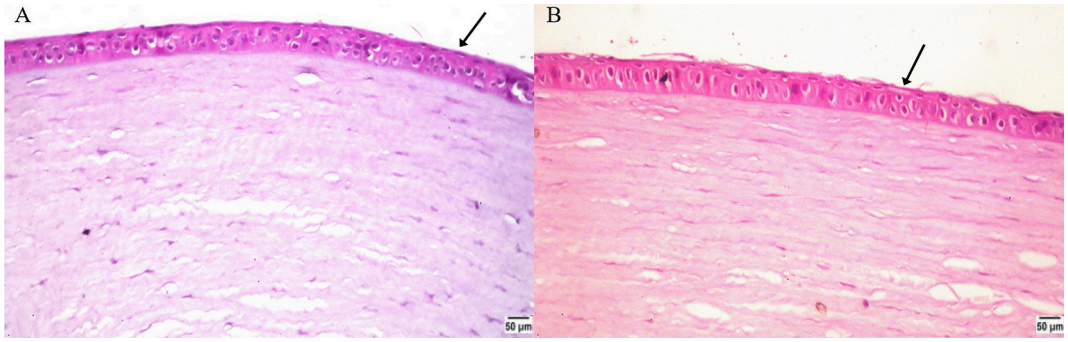

Fig. 4. Photomicrographs of the rabbits' corneas following the instillation of A: Normal saline solution as negative control and B: Optimized TCN-EHE.

in Fig. 3A, the captured TEM micrograph is accentuating perfectly shaped spherical vesicle, whose diameter is aligning with those determined by zetasizer analysis.

3.3.6. *Fourier-transform infra-red spectroscopy (FTIR)*

The FTIR spectra of TCN, Brij® 35, Cholesterol and optimized TCN-EHE are illustrated in Fig. 3B, C, D and E respectively. The FTIR spectrum of TCN included the following characteristic peaks, C = N stretching appeared at 1585.49 cm^{-1}, C = C aromatic stretch band at 1465.90 cm^{-1}, a peak at 1103.28 cm^{-1} corresponding to C-O-C ether stretch band and C-Cl stretch band at 794.67 cm^{-1}. Regarding Brij® 35, aliphatic O-H appeared at 3622.32 cm^{-1}, aliphatic CH_2 and CH_3 bands were shown at 1469.76 cm^{-1} and 1346.31 cm^{-1} respectively and finally, C-O-C peaks appeared at 1280.73 cm^{-1}, 1242.16 cm^{-1} and 1114.86 cm^{-1} (Hanif et al., 2023). As for Cholesterol, a peak corresponding to OH stretch bands appeared at 3433.29, in addition to asymmetric and symmetric stretching bands corresponding to CH_2 and CH_3 groups appeared at 2935.66 cm^{-1}, 2900.94 cm^{-1}, 2866.22 cm^{-1} and 2850.79 cm^{-1} respectively. The vanishing of TCN's characteristics peaks in the FTIR spectrum of TCN-EHE might consolidate the successful drug entrapment inside the optimized system (Ahmed et al., 2022).

3.4. *Safety evaluation*

3.4.1. *pH measurement*

It is imperative to measure pH of the optimized formula to ensure its appropriateness for ocular application. The pH of the optimized formula was 7.20 ± 0.07, since the pH of tear film is 7.4, we could prognosticate the compatibility of the optimized formula for ocular application (Sayed et al., 2021). Furthermore, Mohanty et al. (Mohanty et al., 2013) concluded that a pH ranging from 4 to 8 could improve ocular permeation thus, the pH of the optimized formula is expected to amplify its efficacy.

3.4.2. *Histopathological evaluation*

In evaluating corneal tissue responses, normal saline exposure demonstrated a lack of histopathological alterations, maintaining the integrity of the epithelial cell layer, stromal structure, and endothelium, as depicted in Fig. 4A. Notably, the application of the optimized TCN-EHE displayed unaltered histopathological features across corneal tissues as portrayed in Fig. 4B. Conclusively, the safe application of TCN-EHE to the eye is affirmed, as it avoids any deleterious effects or inflammatory responses (Abdelbary et al., 2016; Ahmed et al., 2025).

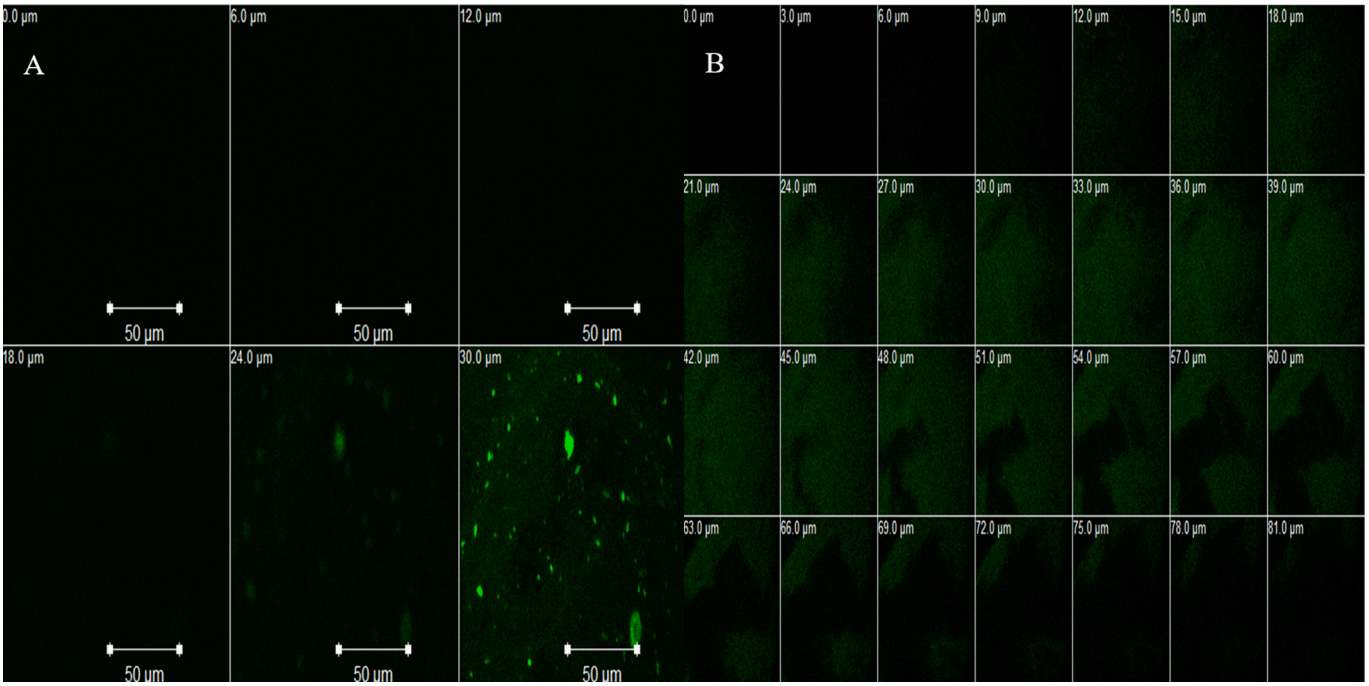

Fig. 5. A: Confocal laser scanning micrographs (CLSM) of rabbits' corneas following the instillation of RhB-solution and B: RhB-EHE optimized formula.

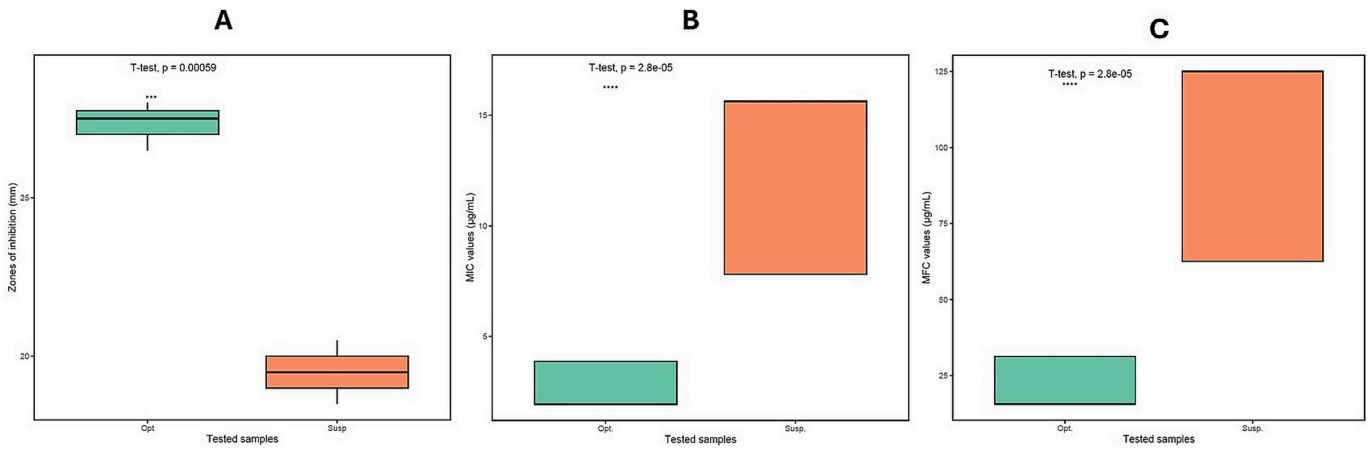

Fig. 6. A: Zone diameter values (mm) of both TCN suspension (Susp.) and the optimized formula (Opt.). B: MIC values (µg/mL) of both TCN suspension (Susp.) and the optimized formula (Opt.). MFC values (µg/mL) of both TCN suspension (Susp.) and the optimized formula (Opt.). Statistical significance was assessed by independent *t*-test, and *p* values are shown.

3.5. 3.5 Efficacy evaluation of the optimized TCN-EHE

3.5.1. In-vivo corneal uptake using confocal laser microscopy (CLM)

Confocal Laser Microscopy (CLM) was utilized to visualize the transcorneal performance of RhB-EHE formulation upon instillation by tracking corneal tissues' emitted fluorescence. The test is to judiciously scrutinize the influence of the optimized formula in enhancing the permeation of TCN through the cornea. Analysis of micrographs revealed notable disparity: the RhB-solution exhibited superficial penetration (30 ± 2 µm) in contrast to the substantially deeper penetration of RhB-EHE optimized formula (81 ± 6 µm) as depicted in Fig. 5A and B respectively. These observations seamlessly align with earlier findings from ex-vivo permeation studies. Enhanced drug permeation could be ascribed to the elastic nature of the prepared TCN-EHE resulted from the use of SAA mixture of hybrid solubility and the addition of edge activator imparting deformable nature to penetrate corneal tissues' tight junctions (El Zaafarany et al., 2010; Kakkar and Kaur, 2011; Younes et al., 2024). The ability of the optimized formula to deliver TCN into the stromal layer presents an auspicious therapeutic avenue for addressing deep-seated fungal ocular infections (Ahmed et al., 2022; Younes et al., 2018).

3.5.2. Antifungal activity determination using disk diffusion susceptibility test

The optimized TCN-EHE showed bigger zone of inhibition (27.03 ± 1.2 mm), when compared to the TCN suspension zone of inhibition (19.7 ± 0.25 mm) as depicted in Fig. 6A. This observation suggested a higher antifungal activity of the optimized TCN-EHE against the tested *Candida albicans* standard strain. The enhanced antifungal activity could be attributed to the enhanced penetration of TCN-EHE caused by the elastic nature, nanosized vesicles and negative surface charge allowing higher drug concentration to reach deeply infected corneal tissues (Kakkar and Kaur, 2011; Mosallam et al., 2021; Nemr et al., 2024). Subsequently, the higher antifungal activity indication was further investigated by MIC determination of both preparations.

3.5.3. Minimum inhibitory concentration (MIC)

To investigate the enhanced activity of the optimized TCN-EHE compared to the tested TCN suspension, minimum fungal inhibitory concentration was determined by broth microdilution technique. The MIC of the optimized formula (1.93 µg/mL) was significantly lower (8-fold) than that of the TCN suspension (15.625 µg/mL), as illustrated in Fig. 6B. Hence, the antifungal activity of TCN was improved by the optimized TCN-EHE in comparison to the TCN suspension owing to better permeation of TCN-EHE as a result of their elastic nature allowing them to squeeze through corneal tissues imparted by the use of hybrid surfactants (Ahmed et al., 2022) and edge activator (Ahmed et al., 2024c; El Zaafarany et al., 2010) in addition to cholesterol as a penetration enhancer (Eldeeb et al., 2019). Thus, confirming disk diffusion susceptibility results. Statistical significance was assessed by independent *t*-test ($P < 0.01$) and the statistics were performed in version 4.1.2 of R (R Core Team, 2022).

In the literature, various nanocarrier systems have been evaluated for terconazole delivery. For example, studies using terconazole-loaded liposomes have reported MIC reductions of 2-, 4-, and 16-fold (Albash et al., 2021; Bahy and Helal, 2022; Mosallam et al., 2021). Formulations based on polymeric nanoparticles or micelles have demonstrated improvements of approximately 1- to 6-fold (Elnaggar et al., 2016; Liang et al., 2021; Mohsen, 2022). Thus, our formulation's 8-fold reduction compares very favorably with other terconazole nanocarriers, suggesting a superior enhancement in antifungal efficacy.

3.5.4. Minimum fungicidal concentration (MFC)

The broth microdilution technique was used to assess MFC for both TCN suspension and the optimized TCN-EHE. Both preparations exhibited fungicidal effect after 24 h of incubation at 37 °C. The optimized TCN-EHE showed a significantly lower (8-fold) MFC at 15.625 µg/mL than the drug suspension whose MFC was 125 µg/mL as shown in Fig. 6C. Hence, the optimized TCN-EHE has higher fungicidal activity when compared to the drug suspension which is coinciding the MIC results, reflecting the enhanced drug penetration through corneal tissues, as previously discussed. The statistics were performed in version 4.1.2 of R (R Core Team, 2022), using independent t-test ($P < 0.01$).

Literature review revealed that various nanocarrier systems have been evaluated for terconazole delivery. Terconazole-loaded liposomes have reported MIC reductions of 2-, 4-, and 16-fold (Albash et al., 2021; Bahy and Helal, 2022; Mosallam et al., 2021). Formulations based on polymeric nanoparticles or micelles have demonstrated improvements of approximately 1- to 6-fold (Elnaggar et al., 2016; Liang et al., 2021; Mohsen, 2022). Thus, our formulation's 8-fold reduction compares very favorably with other terconazole nanocarriers, suggesting a plausible enhancement in antifungal efficacy.

3.5.5. Effect of the optimized TCN-EHE and TCN suspension on the biofilm formation of the tested standard strain

The changes in biofilm formation by the tested standard strain of *Candida albicans* in the presence of TCN (either as TCN suspension or optimized TCN-EHE) were determined by crystal violet assay. The anti-biofilm activity of the optimized TCN-EHE was compared to that of the TCN suspension at concentrations equal to $^1/_8$, ¼, ½, 1, 2, and 4 X, where

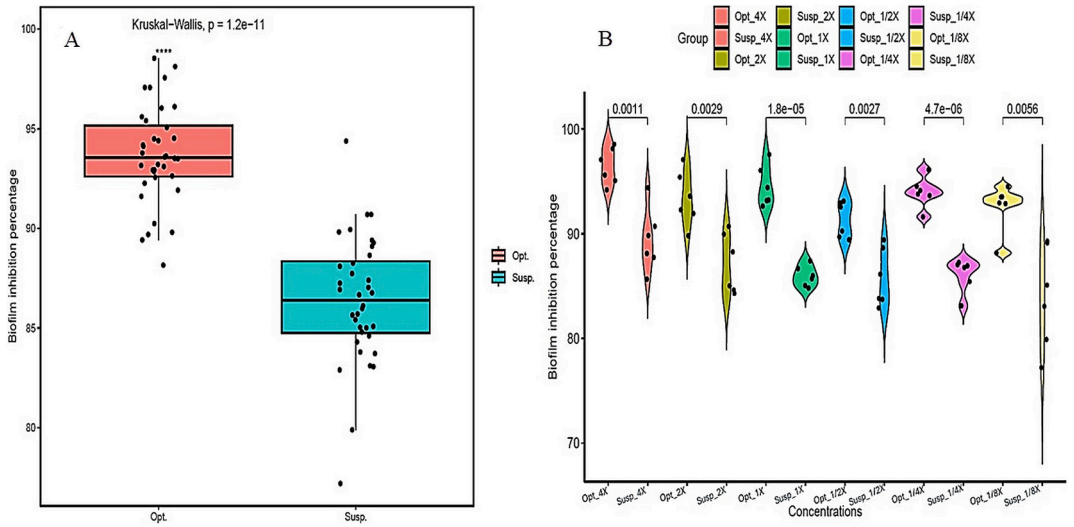

Fig. 7. A: Biofilm inhibition percentage of TCN suspension (Susp.) and the optimized formula (Opt.) of TCN-EHE. Each dot represents a replica of each of the six tested concentrations ($n = 36$ per preparation group). B: Anti-biofilm activity (biofilm inhibition %) against *Candida albicans* standard strain ATCC 60193 at different concentrations.

X is the calculated MIC (7.8125–0.2441 μg/mL) and (62.5–1.95312 μg/mL) for the optimized TCN-EHE and TCN suspension respectively. The optimized TCN-EHE showed significantly higher biofilm inhibition activity than that of the TCN suspension against the tested *Candida albicans* standard strain (Kruskal-Wallis test, $P < 0.01$, Fig. 7A), at all tested concentrations (independent t-test, $P < 0.01$, Fig. 7B). The statistics were performed in version 4.1.2 of R (R Core Team, 2022) and visualized in RStudio (Racine, 2012).

The obtained results suggested that the optimized TCN-EHE significantly ($P < 0.01$) increased the biofilm inhibition activity and enhanced fungicidal activity of TCN, ascribed to the improved permeability through corneal tissues fostered by the elastic nature imparted by using hybrid surfactants and edge activator along with cholesterol as penetration enhancer (Ahmed et al., 2024a; El Zaafarany et al., 2010; Eldeeb et al., 2019). Thus, allowing the disruption of the biofilm integrity and enhancing deeper penetration into the biofilm's dense extracellular matrix. This enhanced penetration allows more effective delivery of terconazole to deeper layers within the biofilm, where cells are often harder to reach and less susceptible to treatment (Aziz et al., 2018). The hybrid elastosome might act synergistically with terconazole to disrupt the cell membranes of fungal cells within the biofilm. This dual-action approach could enhance the biofilm's susceptibility to treatment, leading to more efficient fungicidal effects.

The TCN-EHE formulation could also induce oxidative stress within biofilm-associated fungal cells, potentially leading to cell damage and further enhancing biofilm inhibition. Nanocarrier systems, including elastosomes, have been shown to promote reactive oxygen species (ROS) production, which may play a role in the improved anti-biofilm effect (Sun et al., 2024)

4. Conclusion

Terconazole-loaded edge-activated hybrid elastosomes (TCN-EHE) were successfully formulated using the thin film hydration technique, guided by a D-optimal design to meticulously assess key formulation variables. The optimized formulation (desirability = 0.871) demonstrated remarkable characteristics, including high entrapment efficiency (91.45 ± 2.19 %), nanosized particles confirmed by TEM (232.85 ± 1.48 nm), stable zeta potential (−31.4 ± 0.28 mV), and a biphasic release profile (46.02 % ± 0.09 % at 2 h and 92.83 % ± 3.28 % at 8 h), all of which remained consistent after short-term storage.

Ex-vivo studies revealed a 1.94-fold increase in corneal permeation flux compared to conventional formulations. Corneal hydration, pH, and histopathological analysis confirmed its safety. In vivo imaging via CLM showcased deeper corneal penetration (81 μm) versus a terconazole suspension (30 μm). The optimized TCN-EHE exhibited superior antifungal efficacy, producing a larger zone of inhibition (27.03 ± 1.2 mm *vs.* 19.7 ± 0.25 mm), an eightfold reduction in MIC and MFC, and significantly enhanced biofilm inhibition. These improvements are attributed to the hybrid blend of surfactants, EA and cholesterol, which imparted elasticity to the vesicles, allowing them to traverse the corneal membrane. TCN-EHE holds great promise as an advanced ocular antifungal therapy.

Ethical statements and approval

All ex-vivo and in-vivo experiments were conducted with the approval of the Research Ethics Committee at the Faculty of Pharmacy, Cairo University (Approval No. PI 3505). The study adhered to the guidelines outlined in the Guide for the Care and Use of Laboratory Animals, as issued by the US National Institute of Health (NIH Publication No. 85–23, revised 2011).

CRediT authorship contribution statement

Sadek Ahmed: Writing – review & editing, Supervision, Investigation, Formal analysis, Conceptualization. **Michael M. Farag:** Writing – review & editing, Writing – original draft, Formal analysis. **Heba Attia:** Writing – review & editing, Writing – original draft, Investigation, Formal analysis. **Bander Balkhi:** Supervision, Resources, Conceptualization. **Islam M. Adel:** Supervision, Resources, Investigation. **Asmaa Ashraf Nemr:** Supervision, Resources, Investigation.

Declaration of competing interest

The authors confirm that they have no financial conflicts of interest or personal affiliations that could have potentially influenced the findings presented in this manuscript.

Acknowledgements

Researchers Supporting Project number (RSP2025R76), King Saud University, Riyadh, Saudi Arabia.

Appendix A. Supplementary data

Supplementary data to this article can be found online at https://doi.org/10.1016/j.ijpx.2025.100333.

Data availability

All the data produced or examined in this research are fully presented within this manuscript.

References

Abdelbary, A.A., Abd-Elsalam, W.H., Al-Mahallawi, A.M., 2016. Fabrication of novel ultradeformable bilosomes for enhanced ocular delivery of terconazole: in vitro characterization, ex vivo permeation and in vivo safety assessment. Int. J. Pharm. 513, 688–696.

Abdelbary, G.A., Amin, M.M., Zakaria, M.Y., 2017. Ocular ketoconazole-loaded proniosomal gels: formulation, ex vivo corneal permeation and in vivo studies. Drug Deliv. 24, 309–319.

Abdelhakeem, E., El-Nabarawi, M., Shamma, R., 2021. Effective ocular delivery of eplerenone using nanoengineered lipid carriers in rabbit model. Int. J. Nanomedicine 4985–5002.

Abdelkader, H., Ismail, S., Kamal, A., Alany, R., 2010. Preparation of niosomes as an ocular delivery system for naltrexone hydrochloride: physicochemical characterization. Die Pharmazie An Int. J. Pharmace. Sci. 65, 811–817.

Abdellatif, M.M., Josef, M., El-Nabarawi, M.A., Teaima, M., 2022. Sertaconazole-nitrate-loaded leciplex for treating keratomycosis: optimization using D-optimal design and in vitro, ex vivo, and in vivo studies. Pharmaceutics 14, 2215.

Ahmed, S., Amin, M.M., El-Korany, S.M., Sayed, S., 2022. Corneal targeted fenticonazole nitrate-loaded novasomes for the management of ocular candidiasis: Preparation, in vitro characterization, ex vivo and in vivo assessments. Drug Deliv. 29, 2428–2441.

Ahmed, S., Attia, H., Saher, O., Fahmy, A.M., 2024a. Augmented glycerosomes as a promising approach against fungal ear infection: optimization and microbiological, ex vivo and in vivo assessments. Int. J. Pharm. X, 100295.

Ahmed, S., Aziz, D.E., Sadek, M.A., Tawfik, M.A., 2024b. Capped flexosomes for prominent anti-inflammatory activity: development, optimization, and ex vivo and in vivo assessments. Drug Deliv. Transl. Res. 1–14.

Ahmed, S., Farag, M.M., Sadek, M.A., Aziz, D.E., 2024c. Transdermal application of diacerin loaded-terpene enriched invasomes: an approach to augment anti-edema and nociception inhibition activity. J. Liposome Res. 1–14.

Ahmed, S., Farag, M.M., Attia, H., Balkhi, B., Adel, I.M., Nemr, A.A., 2025. Exploring the potential of antifungal-loaded proniosomes to consolidate corneal permeation in fungal keratitis: a comprehensive investigation from laboratory characterization to microbiological evaluation. Int. J. Pharm. X, 100322.

Al-Badriyeh, D., Leung, L., Davies, G.E., Stewart, K., Kong, D., 2009. Successful use of topical voriconazole 1% alone as first-line antifungal therapy against *Candida albicans* keratitis. Ann. Pharmacother. 43, 2103–2107.

Al-Badriyeh, D., Neoh, C.F., Stewart, K., Kong, D.C., 2010. Clinical utility of voriconazole eye drops in ophthalmic fungal keratitis. Clin. Ophthalmol. 391–405.

Albash, R., Al-Mahallawi, A.M., Hassan, M., Alaa-Eldin, A.A., 2021. Development and optimization of terpene-enriched vesicles (Terpesomes) for effective ocular delivery of fenticonazole nitrate: in vitro characterization and in vivo assessment. Int. J. Nanomedicine 609–621.

Alhakamy, N.A., Hosny, K.M., Rizg, W.Y., Eshmawi, B.A., Badr, M.Y., Safhi, A.Y., Murshid, S.S., 2022. Development and optimization of hyaluronic acid-poloxamer in-situ gel loaded with voriconazole cubosomes for enhancement of activity against ocular fungal infection. Gels 8, 241.

Al-Mahallawi, A.M., Abdelbary, A.A., Aburahma, M.H., 2015. Investigating the potential of employing bilosomes as a novel vesicular carrier for transdermal delivery of tenoxicam. Int. J. Pharm. 485, 329–340.

Al-Mahallawi, A.M., Khowessah, O.M., Shoukri, R.A., 2017. Enhanced non invasive trans-tympanic delivery of ciprofloxacin through encapsulation into nano-spanlastic vesicles: Fabrication, in-vitro characterization, and comparative ex-vivo permeation studies. Int. J. Pharm. 522, 157–164.

Aziz, D.E., Abdelbary, A.A., Elassasy, A.I., 2018. Fabrication of novel elastosomes for boosting the transdermal delivery of diacerein: statistical optimization, ex-vivo permeation, in-vivo skin deposition and pharmacokinetic assessment compared to oral formulation. Drug Deliv. 25, 815–826.

Aziz, D., Mohamed, S.A., Tayel, S., Makhlouf, A., 2022. Enhanced ocular anti-aspergillus activity of tolnaftate employing novel cosolvent-modified spanlastics: formulation, statistical optimization, kill kinetics, ex vivo trans-corneal permeation, in vivo histopathological and susceptibility study. Pharmaceutics 14, 1746.

Aziz, D., Mohamed, S., Tayel, S., Makhlouf, A., 2023. Flexosomes as a promising nanoplatform for enhancing tolnaftate ocular delivery: Formulation, in vitro characterization, statistical optimization, ex vivo and microbial in vivo studies. Int. J. Pharm. 646, 123471.

Bahy, R., Helal, D.A., 2022. Evaluation of the Antimycotic activity of Terconazole proniosomal Gel. Egypt. J. Med. Microbiol. 31, 121–126.

Barbalho, G.N., Brugger, S., Raab, C., Lechner, J.-S., Gratieri, T., Keck, C.M., Rupenthal, I.D., Agarwal, P., 2024. Development of transferosomes for topical ocular drug delivery of curcumin. Eur. J. Pharm. Biopharm. 205, 114535.

Basha, M., Abd El-Alim, S.H., Shamma, R.N., Awad, G.E., 2013. Design and optimization of surfactant-based nanovesicles for ocular delivery of Clotrimazole. J. Liposome Res. 23, 203–210.

Bnyan, R., Khan, I., Ehtezazi, T., Saleem, I., Gordon, S., O'Neill, F., Roberts, M., 2018. Surfactant effects on lipid-based vesicles properties. J. Pharm. Sci. 107, 1237–1246.

Bongomin, F., Gago, S., Oladele, R.O., Denning, D.W., 2017. Global and multi-national prevalence of fungal diseases—estimate precision. J. fungi 3, 57.

Brown, L., Leck, A.K., Gichangi, M., Burton, M.J., Denning, D.W., 2021. The global incidence and diagnosis of fungal keratitis. Lancet Infect. Dis. 21, e49–e57.

Casey-Power, S., Ryan, R., Behl, G., McLoughlin, P., Byrne, M.E., Fitzhenry, L., 2022. Hyaluronic acid: its versatile use in ocular drug delivery with a specific focus on hyaluronic acid-based polyelectrolyte complexes. Pharmaceutics 14, 1479.

Cholkar, K., Dasari, S.R., Pal, D., Mitra, A.K., 2013. Eye: Anatomy, Physiology and Barriers to Drug Delivery, Ocular Transporters and Receptors. Elsevier, pp. 1–36.

CLSI, 2018. Reference Method for Broth Dilution Antifungal Susceptibility Testing of Yeasts; Approved Standard. Clinical and Laboratory Standards Institute, Wayne, PA.

Dai, Y., Zhou, R., Liu, L., Lu, Y., Qi, J., Wu, W., 2013. Liposomes containing bile salts as novel ocular delivery systems for tacrolimus (FK506): in vitro characterization and improved corneal permeation. Int. J. Nanomedicine 1921–1933.

Davies, N.M., 2000. Biopharmaceutical considerations in topical ocular drug delivery. Clin. Exp. Pharmacol. Physiol. 27, 558–562.

Diaz, D.A., Colgan, S.T., Langer, C.S., Bandi, N.T., Likar, M.D., Van Alstine, L., 2016. Dissolution similarity requirements: how similar or dissimilar are the global regulatory expectations? AAPS J. 18, 15–22.

Ding, D., Kundukad, B., Somasundar, A., Vijayan, S., Khan, S.A., Doyle, P.S., 2018. Design of mucoadhesive PLGA microparticles for ocular drug delivery. ACS Appl. Bio Mater. 1, 561–571.

Duangjit, S., Opanasopit, P., Rojanarata, T., Ngawhirunpat, T., 2013. Evaluation of meloxicam-loaded cationic transfersomes as transdermal drug delivery carriers. AAPS PharmSciTech 14, 133–140.

El Taweel, M.M., Tawfik, M.A., Soliman, K., Khattab, M.S., Farag, M.M., 2023. Tailoring of topically applied curcumin loaded pro-novasomes for skin cancer treatment: In-vitro characterization, statistical optimization and histopathological assessment of subcutaneous Ehrlich carcinoma mice model. J. Drug Deliv. Sci. Technol. 88, 104957.

El Zaafarany, G.M., Awad, G.A., Holayel, S.M., Mortada, N.D., 2010. Role of edge activators and surface charge in developing ultradeformable vesicles with enhanced skin delivery. Int. J. Pharm. 397, 164–172.

Eldeeb, A.E., Salah, S., Ghorab, M., 2019. Formulation and evaluation of cubosomes drug delivery system for treatment of glaucoma: ex-vivo permeation and in-vivo pharmacodynamic study. J. Drug Deliv. Sci. Technol. 52, 236–247.

Elgendy, H.A., Makky, A.M., Elakkad, Y.E., Awad, H.H., Hassab, M.A.E., Younes, N.F., 2024. Atorvastatin loaded lecithin-coated zein nanoparticles based thermogel for the intra-articular management of osteoarthritis: in-silico, in-vitro, and in-vivo studies. J. Pharm. Investig. 1–22.

ElMeshad, A.N., Mohsen, A.M., 2016. Enhanced corneal permeation and antimycotic activity of itraconazole against *Candida albicans* via a novel nanosystem vesicle. Drug Deliv. 23, 2115–2123.

Elnaggar, Y.S., Talaat, S.M., Bahey-El-Din, M., Abdallah, O.Y., 2016. Novel lecithin-integrated liquid crystalline nanogels for enhanced cutaneous targeting of terconazole: development, in vitro and in vivo studies. Int. J. Nanomedicine 5531–5547.

Exerowa, D., 1969. Effect of adsorption, ionic strength and p H on the potential of the diffuse electric layer. Kolloid Z. Z. Polym. 232, 703–710.

Fahmy, A.M., Balkhi, B., Sadek, M.A., ElBishbishy, R.M., Ahmed, S., 2025 Apr. PEGylated terpesomes of curcumin for prominent hepatoprotective activity: fabrication, optimization, biochemical analysis and in vivo evaluation. J. Drug Deliv. Sci. Technol. 1, 106876.

Farag, M.M., Abd El Malak, N.S., Yehia, S.A., Ahmed, M.A., 2021. Hyaluronic acid conjugated metformin-phospholipid sonocomplex: a biphasic complexation approach to correct hypoxic tumour microenvironment. Int. J. Nanomedicine 1005–1019.

Farag, M.M., El-Nassan, H.B., Merey, H.A., Eltanany, B.M., Galal, M.M., Wadie, W., El-Tanbouly, D.M., Khattab, M.A., Rashed, L.A., ElMeshad, A.N., 2023. Comparative pharmacodynamic study delineating the efficacy of amantadine loaded nano-emulsified organogel via intranasal versus transdermal route in rotenone-induced Parkinson's disease rat model. J. Drug Deliv. Sci. Technol. 86, 104765.

Farag, M.M., El-Sebaie, W., Basalious, E.B., El-Gazayerly, O.N., 2024. Self-nanoemulsifying/self-assembled cubic nanoparticles lyophilized tablet: a novel biphasic release approach to enhance the bioavailability of a lipophilic Drug. AAPS Pharm. Sci. Tech. 25, 250.

Gaudana, R., Ananthula, H.K., Parenky, A., Mitra, A.K., 2010. Ocular drug delivery. AAPS J. 12, 348–360.

Gonzalez-Pizarro, R., Silva-Abreu, M., Calpena, A.C., Egea, M.A., Espina, M., García, M. L., 2018. Development of fluorometholone-loaded PLGA nanoparticles for treatment of inflammatory disorders of anterior and posterior segments of the eye. Int. J. Pharm. 547, 338–346.

Gorjian, H., Amiri, Z.R., Milani, J.M., Khaligh, N.G., 2021. Preparation and characterization of the encapsulated myrtle extract nanoliposome and nanoniosome without using cholesterol and toxic organic solvents: a comparative study. Food Chem. 342, 128342.

Habib, B.A., Sayed, S., Elsayed, G.M., 2018. Enhanced transdermal delivery of ondansetron using nanovesicular systems: fabrication, characterization, optimization and ex-vivo permeation study-Box-Cox transformation practical example. Eur. J. Pharm. Sci. 115, 352–361.

Haney, E.F., Trimble, M.J., Hancock, R.E.W., 2021. Microtiter plate assays to assess antibiofilm activity against bacteria. Nat. Protoc. 16, 2615–2632.
Hanif, R., Khan, M.I., Madni, A., Akhtar, M.F., Sohail, M.F., Saleem, A., Rehman, M., Usmani, S.J., Khan, A., Masood, A., 2023. Polyoxyethylene lauryl ether (Brij-35) and poloxamer 407–based non-ionic surfactant vesicles for dissolution enhancement of tacrolimus. J. Pharm. Innov. 18, 1487–1499.
Harisa, G.I., Badran, M.M., 2015. Simvastatin nanolipid carriers decreased hypercholesterolemia induced cholesterol inclusion and phosphatidylserine exposure on human erythrocytes. J. Mol. Liq. 208, 202–210.
Huang, J., Peng, T., Li, Y., Zhan, Z., Zeng, Y., Huang, Y., Pan, X., Wu, C.-Y., Wu, C., 2017. Ocular cubosome drug delivery system for timolol maleate: preparation, characterization, cytotoxicity, ex vivo, and in vivo evaluation. AAPS PharmSciTech 18, 2919–2926.
Hussein, A., El-Kayal, M., Shamma, R.N., Awad, H.H., Younes, N.F., 2024. Optimizing nutraceutical-loaded trehalosomes in-situ gel for diabetic cataract management: Comprehensive in vitro and in vivo evaluations. J. Drug Deliv. Sci. Technol. 102, 106368.
Jayachandran, A.L., Katragadda, R., Ravinder, T., Vajravelu, L., Manorajan, L., Hemalatha, S., Shanmugam, K., 2018. Antifungal susceptibility pattern among candida species: an evaluation of disc diffusion and micro broth dilution method. J. Microbiol. Infect. Dis. 8, 97–102.
Jesus, J.I., Lourenço, F.R., Ishida, K., Barreto, T.L., Avino, V.C., Neto, E.D., Bou-Chacra, N.A., 2022. Besifloxacin nanocrystal: towards an innovative ophthalmic preparation. Pharmaceutics 14 (10), 2221.
Kakkar, S., Kaur, I.P., 2011. Spanlastics—a novel nanovesicular carrier system for ocular delivery. Int. J. Pharm. 413, 202–210.
Kakkar, S., Pal Kaur, I., 2013. A novel nanovesicular carrier system to deliver drug topically. Pharm. Dev. Technol. 18, 673–685.
Karraker, K., Radke, C., 2002. Disjoining pressures, zeta potentials and surface tensions of aqueous non-ionic surfactant/electrolyte solutions: theory and comparison to experiment. Adv. Colloid Interf. Sci. 96, 231–264.
Kouchak, M., Mahmoodzadeh, M., Farrahi, F., 2019. Designing of a pH-triggered Carbopol®/HPMC in situ gel for ocular delivery of dorzolamide HCl: in vitro, in vivo, and ex vivo evaluation. AAPS PharmSciTech 20, 1–8.
Leck, A., Thomas, P., Hagan, M., Kaliamurthy, J., Ackuaku, E., John, M., Newman, M., Codjoe, F., Opintan, J., Kalavathy, C., 2002. Aetiology of suppurative corneal ulcers in Ghana and South India, and epidemiology of fungal keratitis. Br. J. Ophthalmol. 86, 1211–1215.
Liang, Z., Zhang, Z., Yang, J., Lu, P., Zhou, T., Li, J., Zhang, J., 2021. Assessment to the antifungal effects in vitro and the ocular pharmacokinetics of solid-lipid nanoparticle in rabbits. Int. J. Nanomedicine 7847–7857.
Liang, Z., Zhang, Z., Lu, P., Yang, J., Han, L., Liu, S., Zhou, T., Li, J., Zhang, J., 2023. The effect of charges on the corneal penetration of solid lipid nanoparticles loaded Econazole after topical administration in rabbits. Eur. J. Pharm. Sci. 187, 106494.
Liu, Z., Pan, W., Nie, S., Zhang, L., Yang, X., Li, J., 2005. Preparation and evaluation of sustained ophthalmic gel of enoxacin. Drug Dev. Ind. Pharm. 31, 969–975.
Liu, Z., Zhang, X., Wu, H., Li, J., Shu, L., Liu, R., Li, L., Li, N., 2011. Preparation and evaluation of solid lipid nanoparticles of baicalin for ocular drug delivery system in vitro and in vivo. Drug Dev. Ind. Pharm. 37, 475–481.
Mahale, N., Thakkar, P., Mali, R., Walunj, D., Chaudhari, S., 2012. Niosomes: novel sustained release nonionic stable vesicular systems—an overview. Adv. Colloid Interf. Sci. 183, 46–54.
Mannermaa, E., Vellonen, K.-S., Urtti, A., 2006. Drug transport in corneal epithelium and blood–retina barrier: emerging role of transporters in ocular pharmacokinetics. Adv. Drug Deliv. Rev. 58, 1136–1163.
Manosroi, A., Wongtrakul, P., Manosroi, J., Sakai, H., Sugawara, F., Yuasa, M., Abe, M., 2003. Characterization of vesicles prepared with various non-ionic surfactants mixed with cholesterol. Colloids Surf. B: Biointerfaces 30, 129–138.
Mohanty, B., Mishra, S.K., Majumdar, D.K., 2013. Effect of formulation factors on in vitro transcorneal permeation of voriconazole from aqueous drops. J. Adv. Pharm. Technol. Res. 4, 210–216.
Mohsen, A.M., 2022. Cationic polymeric nanoparticles for improved ocular delivery and antimycotic activity of terconazole. J. Pharm. Sci. 111, 458–468.
Mosallam, S., Ragaie, M.H., Moftah, N.H., Elshafeey, A.H., Abdelbary, A.A., 2021. Use of novasomes as a vesicular carrier for improving the topical delivery of terconazole: in vitro characterization, in vivo assessment and exploratory clinical experimentation. Int. J. Nanomedicine 119–132.
Moustafa, M.A., Elnaggar, Y.S., El-Refaie, W.M., Abdallah, O.Y., 2017. Hyalugel-integrated liposomes as a novel ocular nanosized delivery system of fluconazole with promising prolonged effect. Int. J. Pharm. 534, 14–24.
Nemr, A.A., Ahmed, S., Adel, I.M., 2024. Limonene-enriched ultra-structural cubosomes to augment ocular delivery of a poorly water soluble anti-fungal drug: Fabrication, characterization, statistical optimization, in vivo corneal uptake and histopathological evaluation in rabbits. J. Drug Deliv Sci. Technol. 98, 105886.
Nemr, A.A., El-Mahrouk, G.M., Badie, H.A., 2021. Development and evaluation of proniosomes to enhance the transdermal delivery of cilostazole and to ensure the safety of its application. Drug Dev. Ind. Pharm. 47, 403–415.
Nemr, A.A., El-Mahrouk, G.M., Badie, H.A., 2022. Development and evaluation of surfactant-based elastic vesicular system for transdermal delivery of Cilostazole: ex-vivo permeation and histopathological evaluation studies. J. Liposome Res. 32, 159–171.
Nemr, A.A., El-Mahrouk, G.M., Badie, H.A., 2023. Enhancement of ocular anti-glaucomic activity of agomelatine through fabrication of hyaluronic acid modified-elastosomes: formulation, statistical optimisation, in vitro characterisation, histopathological study, and in vivo assessment. J. Microencapsul. 40, 423–441.
Osman, E.O., Attia, H., Samir, R., Mahmoud, Z., 2023. Design, synthesis, and antibacterial activity of a new series of ciprofloxacin-thiadiazole hybrid. J. Mol. Struct. 1282, 135135.
O'Toole, GA., 2011. Microtiter dish biofilm formation assay. J. Vis. Expe.: JoVE 30 (47), 2437.
Pardakhty, A., Varshosaz, J., Rouholamini, A., 2007. In vitro study of polyoxyethylene alkyl ether niosomes for delivery of insulin. Int. J. Pharm. 328, 130–141.
Pharmacopeia, U., 2021. 771 Ophthalmic Products—Quality Tests. USP.
Qiao, G.L., Ling, J., Wong, T., Yeung, S.N., Iovieno, A., 2020. Candida keratitis: epidemiology, management, and clinical outcomes. Cornea 39, 801–805.
Quinteros, D.A., Ferreira, L.M., Schaffazick, S.R., Palma, S.D., Allemandi, D.A., Cruz, L., 2016. Novel polymeric nanoparticles intended for ophthalmic administration of acetazolamide. J. Pharm. Sci. 105, 3183–3190.
R Core Team, 2022. R: A Language and Environment for Statistical Computing. R Foundation for Statistical Computing, Vienna, Austria.
Racine, J.S., 2012. RStudio: A Platform-Independent IDE for R and Sweave. JSTOR.
Rathod, S., Arya, S., Shukla, R., Ray, D., Aswal, V.K., Bahadur, P., Tiwari, S., 2021. Investigations on the role of edge activator upon structural transitions in Span vesicles. Colloids Surf. A Physicochem. Eng. Asp. 627, 127246.
Sánchez-López, E., Egea, M., Cano, A., Espina, M., Calpena, A., Ettcheto, M., Camins, A., Souto, E.B., Silva, A.M., García, M.L., 2016. PEGylated PLGA nanospheres optimized by design of experiments for ocular administration of dexibuprofen—in vitro, ex vivo and in vivo characterization. Colloids Surf. B: Biointerfaces 145, 241–250.
Sayed, S., Abdelmoteleb, M., Amin, M.M., Khowessah, O.M., 2020. Effect of formulation variables and gamma sterilization on transcorneal permeation and stability of proniosomal gels as ocular platforms for antiglaucomal drug. AAPS Pharm. Sci. Tech. 21, 1–13.
Sayed, S., Abdel-Moteleb, M., Amin, M.M., Khowessah, O.M., 2021. Cubogel as potential platform for glaucoma management. Drug Deliv. 28, 293–305.
Shahab, M.S., Rizwanullah, M., Alshehri, S., Imam, S.S., 2020. Optimization to development of chitosan decorated polycaprolactone nanoparticles for improved ocular delivery of dorzolamide: in vitro, ex vivo and toxicity assessments. Int. J. Biol. Macromol. 163, 2392–2404.
Shakeel, F., Baboota, S., Ahuja, A., Ali, J., Aqil, M., Shafiq, S., 2007. Nanoemulsions as vehicles for transdermal delivery of aceclofenac. AAPS Pharm. Sci. Tech. 8, 191–199.
Shang, H., Younas, A., Zhang, N., 2022. Recent advances on transdermal delivery systems for the treatment of arthritic injuries: from classical treatment to nanomedicines. Wiley Interdiscip. Rev. Nanomed. Nanobiotechnol. 14, e1778.
Singh, A., Singh, D., Kumar, S., Mishra, A., Verma, R., Mishra, V., 2015. A retrospective study of fungal corneal ulcer from the western part of Uttar Pradesh. Int. J. Res. Med. Sci. 3, 880.
Srivastava, V., Singh, V., Khatri, D.K., Mehra, N.K., 2023. Recent trends and updates on ultradeformable and elastic vesicles in ocular drug delivery. Drug Discov. Today 28, 103647.
Sun, N., Jiang, X., Meng, Q., Jiang, H., Yuan, Z., Zhang, J., 2024. Preparation of nanoparticles loaded with quercetin and effects on bacterial biofilm and LPS-induced oxidative stress in *Dugesia japonica*. Appl. Biochem. Biotechnol. 196, 32–49.
Tawfik, M.A., Eltaweel, M.M., Farag, M.M., Shamsel-Din, H.A., Ibrahim, A.B., 2023. Sonophoresis-assisted transdermal delivery of antimigraine-loaded nanolipomers: Radio-tracking, histopathological assessment and in-vivo biodistribution study. Int. J. Pharm. 644, 123338.
Taymouri, S., Varshosaz, J., 2016. Effect of different types of surfactants on the physical properties and stability of carvedilol nano-niosomes. Adv. Biomed. Res. 5, 48.
Weng, J., Tong, H.H., Chow, S.F., 2020. In vitro release study of the polymeric drug nanoparticles: development and validation of a novel method. Pharmaceutics 12, 732.
Whitcher, J.P., Srinivasan, M., Upadhyay, M.P., 2001. Corneal blindness: a global perspective. Bull. World Health Organ. 79, 214–221.
Younes, N.F., Abdel-Halim, S.A., Elassasy, A.I., 2018. Corneal targeted Sertaconazole nitrate loaded cubosomes: preparation, statistical optimization, in vitro characterization, ex vivo permeation and in vivo studies. Int. J. Pharm. 553, 386–397.
Younes, N.F., Sayed, S., Hassan, M., Ahmed, S., 2024. Engineered lecithin-based proniosomes for enhanced trans-tympanic permeation: in vitro, microbiological, ex vivo and in vivo evaluation. J. Drug Deliv. Sci. Technol. 96, 105728.
Yousry, C., Zikry, P.M., Salem, H.M., Basalious, E.B., El-Gazayerly, O.N., 2020. Integrated nanovesicular/self-nanoemulsifying system (INV/SNES) for enhanced dual ocular drug delivery: statistical optimization, in vitro and in vivo evaluation. Drug Deliv. Transl. Res. 10, 801–814.
Zaghloul, N., El Hoffy, N.M., Mahmoud, A.A., Elkasabgy, N.A., 2022a. Cyclodextrin stabilized freeze-dried silica/chitosan nanoparticles for improved terconazole ocular bioavailability. Pharmaceutics 14, 470.
Zaghloul, N., Mahmoud, A.A., Elkasabgy, N.A., El Hoffy, N.M., 2022b. PLGA-modified Syloid®-based microparticles for the ocular delivery of terconazole: in-vitro and in-vivo investigations. Drug Deliv. 29, 2117–2129.